

The importance of harmonic versus random excitation for a human finger

Janko Slavič^{a,*}, Luka Knez^a, Miha Boltežar^a

^a *University of Ljubljana, Faculty of Mechanical Engineering, Aškerčeva 6, 1000 Ljubljana, Slovenia*

Cite as:

**Janko Slavič, Luka Knez and Miha Boltežar,
The importance of harmonic versus random excitation for a human
finger,
International Journal of Mechanical Sciences, 2017,
DOI: 10.1016/j.ijmecsci.2017.08.017**

Abstract

In hand-held devices the vibration excitation is typically multi-harmonic (e.g., as a result of the eccentricity in rotating motors) on top of the random excitation. The excitation amplitude, excitation frequency and the push force typically vary with the application or the usage conditions. Typically, random excitation is used for finger or hand excitation. This paper investigates the importance of harmonic versus random excitation for a human index finger. Under different testing conditions the finger's response was researched via the apparent mass. The harmonic excitation was studied using a sine sweep profile where the continuous wavelet transform was used for the extraction of the instantaneous apparent mass. The results show significant differences in the identified apparent mass for harmonic excitation when compared to random excitation (e.g., at frequencies close to 10 Hz the apparent mass was up to 3 times higher for a random excitation than for a harmonic excitation).

As hand tools are frequently excited with a single or multiple harmonics, the identified differences should help in the process of designing safer hand tools.

Keywords: Continuous wavelet transform, apparent mass of a finger, random and harmonic excitation, nonlinearity, biodynamics

*Corresponding author: janko.slavic@fs.uni-lj.si, +386 1 4771 226, fax:+386 1 2518 567

1. Introduction

Prolonged exposure of the human hand-arm system to vibration leads to vibration-induced injuries [1, 2]. Exposure to vibration is typically researched via the so-called biodynamic response parameters [1], i.e., the apparent mass, the mechanical impedance or the apparent stiffness, which are obtained by dividing the dynamic force by the acceleration, the velocity or the displacement, respectively. For the sake of repeatability, these biodynamic response parameters are usually measured with a vibrating handle, which simulates the hand-tool excitations and measures the grip and push forces [3, 4, 5]. The handle can simulate the broadband random noise or the harmonic excitation.

To obtain the dynamic response parameters of a human hand-arm system a standardized [6] or the driving-point, biodynamic response method [7, 8, 9] can be used. While the standard approach requires an acceleration sensor between the hand and the handle [8], the driving-point biodynamic approach is based on the acceleration and the force applied to the handle. Without an additional sensor between the handle and the hand, the driving-point biodynamic approach is much easier to use, more reliable, but requires a mass correction due to the mass of the handle [7].

Vibration injuries are often localized in the palm or in parts of the fingers [10, 11]; therefore, the biodynamic response method has recently been improved by Dong *et al.* [12]. The handle researched in [12] measured the total acceleration and the forces on all five fingers. Analyses of the results found that the responses of the fingers are different compared to that of the hand. In an effort to investigate the relative motion and the vibration transmissibility of the fingers, Concettoni and Griffin [13] replaced the traditional instrument handle with a flat metal plate.

The biodynamic response is usually researched during broadband random excitation [14, 15, 16]. However, besides broadband random excitation, most hand-held tools are also harmonically excited. Hand-held or other tools usually use rotating motors or reciprocating engines that are a source of single- or multi-harmonic excitation. With a change of the rotating speed, the harmonic excitation frequency changes. If broadband and harmonic excitations at the same RMS (root-mean-square) values are compared, the energy during harmonic excitation is focused on a narrow frequency, and therefore significant differences are expected.

Research on harmonic excitation of the hand-arm system has focused on a constant acceleration amplitude or a constant frequency, e.g., see [17, 18, 19, 20]. Gurram *et al.* [18] researched the importance of sine versus broadband excitation of a hand-arm system and found significant differences.

This study focuses on an index finger subjected to broadband random and harmonic sine-sweep excitation under various testing conditions. With the sine-sweep, the excitation frequency is continuously changing, which makes the classic approach based on auto and cross spectra difficult to implement. Therefore, to identify the sine-sweep apparent mass, this research applies the continuous wavelet transform [21, 22, 23]. Different excitation types, acceleration ampli-

tudes and sine-sweep rates were tested and the influence of the push force on the index finger's response was also researched.

The paper is organized as follows. Basic overviews of the biodynamic theory and the continuous wavelet transform are presented in Section 2 as well as the identification of the finger's apparent mass and the push force. The experimental setup and the testing conditions are described in Section 3. To ensure the validity of the measured data a dynamic characterization of the measuring device was also made. The finger's apparent masses for both types of excitation are presented in Section 4 and the findings of the study are discussed in Section 5 and highlighted in the conclusions in Section 6.

2. Theoretical background

2.1. Biodynamic theory

A brief overview of the biodynamic response theory is presented in this section. The theory is then used to derive the biodynamic response of the index finger that is investigated in this study. For details the reader is referred to Griffin [1] and Dong et al. [7].

The response of any biodynamic system is characterised by the biodynamic response parameters: either the apparent mass, the mechanical impedance or the apparent stiffness [1, 7]:

$$AM = \frac{F}{A}, \quad MI = \frac{F}{V}, \quad AS = \frac{F}{D}, \quad (1)$$

where F , A , V , D are the force, acceleration, velocity and displacement at the hand driving-point, respectively. The apparent mass estimator \widetilde{AM} is obtained in the frequency domain by performing [7]:

$$\widetilde{AM}(\omega) = \frac{G_{fa}(\omega)}{G_{aa}(\omega)}, \quad (2)$$

where G_{fa} is the cross-spectrum density of the force and the acceleration and G_{aa} is the auto-spectrum density of the acceleration. The apparent mass is a complex number as both G_{fa} and G_{aa} are complex values.

Every sensor used in the measurement has a certain amount of mass. Hence, the measured force of the finger is in fact a combination of the finger's biodynamic force and the inertial force of the measuring device. To calculate the pure apparent mass of the index finger $\widetilde{AM}_{\text{Finger}}$ it is therefore necessary to deduct the effect of the measuring device $\widetilde{AM}_{\text{Device}}$:

$$\widetilde{AM}_{\text{Finger}}(\omega) = \widetilde{AM}_{\text{FingerDev}}(\omega) - \widetilde{AM}_{\text{Device}}(\omega), \quad (3)$$

where $\widetilde{AM}_{\text{FingerDev}}$ is the combined apparent mass of the device and the finger. The $\widetilde{AM}_{\text{Device}}$ in Eq. (3) was obtained from the data measured on an empty measuring device. Since there is no finger pushing down on the device, the dynamic force signal is purely the result of the measuring device's mass.

To obtain the static push force component $F_p(t)$, the measured samples were averaged in the time domain (the averaging period was 0.5 s):

$$F_p(t) = \text{Mean}(F(t)). \quad (4)$$

2.2. Continuous wavelet transform

With sine-sweep testing, the frequency changes and the apparent mass at the current excitation frequency were estimated using the Continuous Wavelet Transform (CWT) [21, 23, 24]. For reasons of completeness, the basics of the CWT will be presented here.

The CWT is based on the mother wavelet function $\psi(t)$, which must have a zero mean value:

$$\int_{-\infty}^{+\infty} \psi(t) dt = 0 \quad (5)$$

and has to be normalized:

$$\|\psi(t)\|^2 = \int_{-\infty}^{+\infty} |\psi(t)|^2 dt = 1 \quad (6)$$

The mother wavelet function $\psi(t)$ is translated in time u and scaled with $s > 0$ to obtain the family of wavelet functions $\psi_{u,s}(t)$:

$$\psi_{u,s}(t) = \frac{1}{\sqrt{s}} \psi\left(\frac{t-u}{s}\right). \quad (7)$$

The continuous wavelet transform of a function $x(t)$ can now be defined as:

$$Wx(u, s) = \int_{-\infty}^{+\infty} x(t) \psi_{u,s}^*(t) dt, \quad (8)$$

where $\psi_{u,s}^*(t)$ is the complex conjugate of the wavelet $\psi_{u,s}(t)$. The scale s and the angular velocity $\omega(s)$ are related via the frequency modulation η as: $\omega(s) = \eta/s$.

Different mother wavelets can be used, and here the Gabor wavelet will be used:

$$\psi_{Gabor}(t) = \frac{1}{(\sigma^2 \pi)^{1/4}} e^{-t^2/(2\sigma^2)} e^{i\eta t}. \quad (9)$$

The parameter σ denotes the width of the Gaussian window of the Gabor wavelet. If $\sigma = 1$ is chosen, the Gabor wavelet becomes identical to the Morlet wavelet. When choosing the appropriate values for the parameters σ and η it is important to have the proper time/frequency resolution and have the edge effect under control [25].

Using the CWT, the apparent mass is identified from the ridge of the CWT [24]:

$$AM(u, s) = \frac{WF(u, s)}{WA(u, s)}. \quad (10)$$

3. The experiment

3.1. Experimental setup

The developed single-finger measurement device together with the operator's index finger are shown in Figure 1. An accelerometer type PCB T333B30 was attached inside the finger-support rectangle from the bottom side using adhesive. The finger-support rectangle is made of aluminium and screwed onto a Kistler 9317B force sensor with M 4 screws. The force sensor is then screwed onto the aluminium base, which is attached to the electrodynamic LDS V555 shaker.

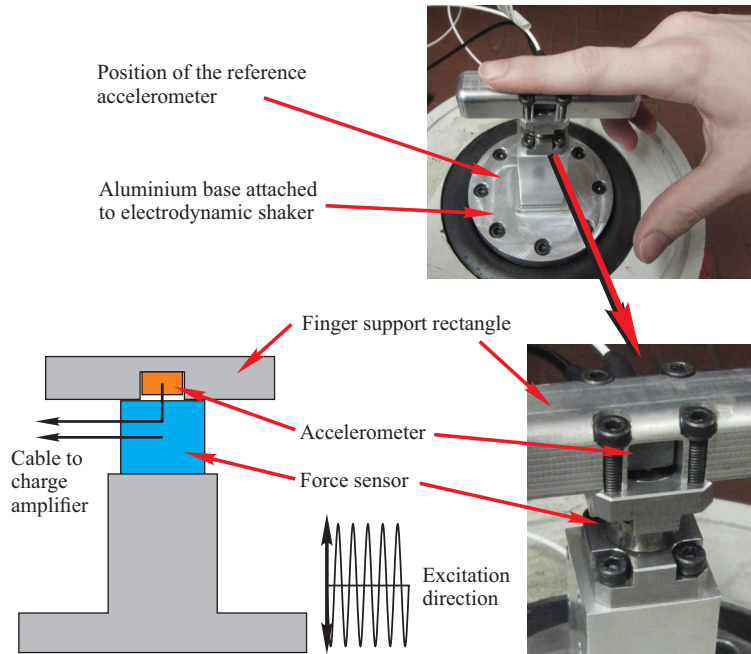


Figure 1: Measuring device with the operator's index finger on the finger-support rectangle. Key components: electrodynamic shaker, force sensor, 2 accelerometers.

The experimental setup used in this study is illustrated in Figure 2. A Kistler 3-axis force sensor type 9317B is used; however, in this research only the excitation direction was measured. The piezoelectric force transducer with the Kistler 5073 charge amplifier can measure the dynamic as well as the quasi-static forces that are applied on the finger-support rectangle. The dynamic component of the force is used for the apparent mass calculations and the static component is displayed to the operator for the pushing-force adjustments during the testing. To measure the accelerations of the finger an accelerometer type PCB T333B30 was used. The accelerometer was attached to the middle of the finger-support rectangle, see Figure 1. Another PCB T333B30 accelerometer was attached to the bottom of the aluminium base to provide the reference for the vibration-feedback control.

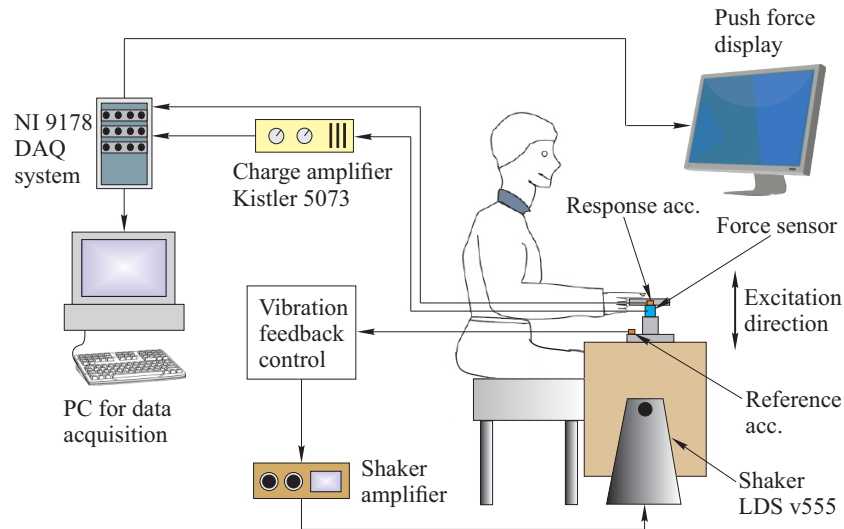


Figure 2: Experimental setup for measurements of the finger's apparent mass.

The measurement data were acquired at a sampling rate of 10 kHz using a National Instruments 9234 acquisition module and the National Instruments 9178 DAQ system. All of the signals were filtered with an analog low-pass filter at a cut-off frequency of 1000 Hz. The National Instruments LabVIEW software served for data acquisition to the PC, and Matlab and Python software were then used for the data analyses.

The measuring device's dynamic properties were determined using modal testing [26] and the first resonance frequency was found at 1145 Hz. The apparent mass of the empty measuring device is shown in Figure 3. The broadband random and the harmonic 4 oct/min sine-sweep excitation profiles had a RMS acceleration value of 10 m/s^2 . As can be seen from Figure 3 the magnitudes of the apparent mass and the phases of the measuring device are, as expected, approximately constant for both types of excitation and correspond to the static mass of the device, which is about 128 g.

3.2. Testing conditions and signal processing

Two types of excitations with varying parameters were used in this study:

- Broadband random excitation in the range from 5 to 250 Hz¹ with a RMS acceleration value of 5 m/s^2 , 10 m/s^2 and 20 m/s^2 .
- Harmonic excitation in the range from 5 to 250 Hz with a RMS acceleration value of 5 m/s^2 , 10 m/s^2 and 20 m/s^2 . The sweep rates used were 2 oct/min, 4 oct/min and 8 oct/min.

¹Dominant components of the vibration for vibration-induced injury lie below 250 Hz [27].

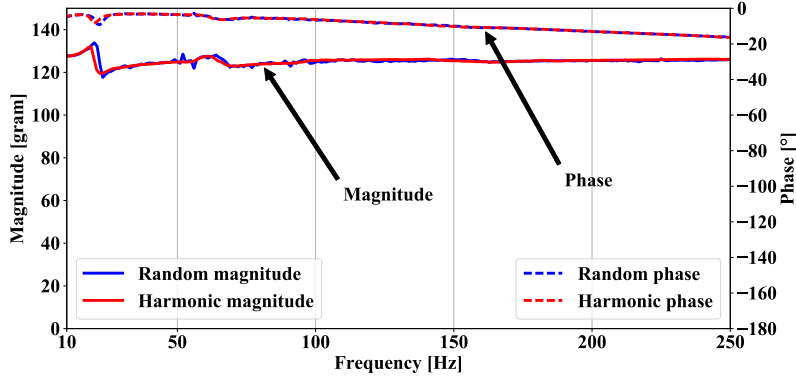


Figure 3: Response of the unloaded experimental setup (no finger), presented in the form of the apparent mass.

For both excitation types the push force varied from 2 N to 10 N with a 1 N step and an additional measurement was made at 15 N.

The operator was seated adjacent to the shaker and the angle of the elbow was held at 90° [15]. The operator pushed down on the measuring rectangle with the right-hand index finger and the forearm was pronated. The lower and upper push-force amplitudes were determined during testing; 2 N was the minimum force that could be reliably exerted by the index finger and forces above 15 N proved hard to hold constant during the longer 2 oct/min sine-sweep measurements. The measurement was repeated five times for each testing condition, resulting in a total of 230 measurements.

The index finger's apparent mass was identified as described in Section 2. The measured force and acceleration signals for the broadband random excitation were transformed into the frequency domain using the Fourier transform (Hamming window; sampling frequency 10 kHz; 20000 samples per segment; 50% overlap). The frequency-domain forces and accelerations were used to calculate the segments of the apparent mass, which were then linearly averaged.

For the harmonic excitation the transformation of the measured forces and accelerations into the frequency domain was made using the continuous wavelet transform (sampling frequency 10 kHz; $\eta = 1$ Hz; $s = 1$). Figure 4 shows a typical spectrogram during harmonic excitation with a sweep sine at 4 oct/min. The CWT ridge of force measurement $WF(u, s)$ and the CWT ridge of the acceleration measurement $WA(u, s)$ were used to identify the apparent mass using Eq. (10).

4. Results

Here, the results for a single person with regards to the excitation types and amplitudes, the sine-sweep rate and the push force will be presented.

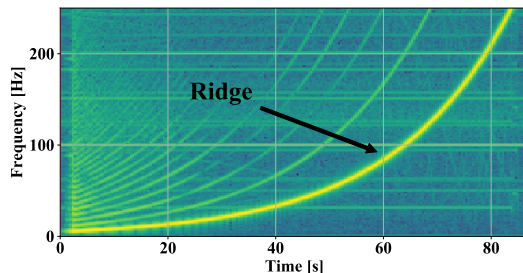


Figure 4: The ridge at sweep-sine excitation: 4 oct/min data, 5 N, RMS 10.

The repeatability of the measured apparent mass was validated first for the broadband random and harmonic excitations, as shown in Figure 5. The RMS acceleration for the random and harmonic 4 oct/min sine-sweep types of excitation was 10 m/s^2 and the finger's push force was 5 N. Each apparent mass magnitude graph was split into two frequency areas: the 10 Hz to 50 Hz with a range up to 300 gram and the 50 Hz to 250 Hz with a range up to 30 g. For the sake of consistency the phase graphs were split in the same frequency areas.

As is evident from Figure 5 the mean apparent mass provides a satisfactory overlap of the individual measurements and is therefore suitable for an influential parameter study. The double standard deviation $2 \cdot \sigma$ values are also displayed and 95% of the measurements lie inside this band.

4.1. The effects of excitation types and amplitudes

Figure 6 shows the apparent mass obtained with broadband random excitation and the apparent mass obtained with the harmonic excitation (the sweep rate was 4 oct/min). Both excitation profiles were measured at three different acceleration amplitudes (5 m/s^2 , 10 m/s^2 and 20 m/s^2) and the push force exerted by the operator was 5 N.

As can be seen from Figure 6 the general shape of the graphs is similar for both the magnitude and the phase: the magnitude values drop rapidly with frequency and the phase values range from -120° to -60° . The apparent-mass magnitudes at a frequency of 10 Hz are relatively high for both excitation types compared to the static mass of the operator's index finger, which was approximately calculated at 58 g using the literature [28].

The difference between the measured and expected apparent-mass values can be explained by the added apparent mass of the hand that is indirectly measured: the operator only placed the index finger on the measuring device, while the palm and possibly other fingers also partially influenced the results. This influence is prominent for the lower frequencies and reduced at higher frequencies, where only a small portion of the vibration is transmitted beyond the finger itself. It has proven difficult to experimentally determine exactly how much apparent mass is added to the measured results at the lower frequencies.

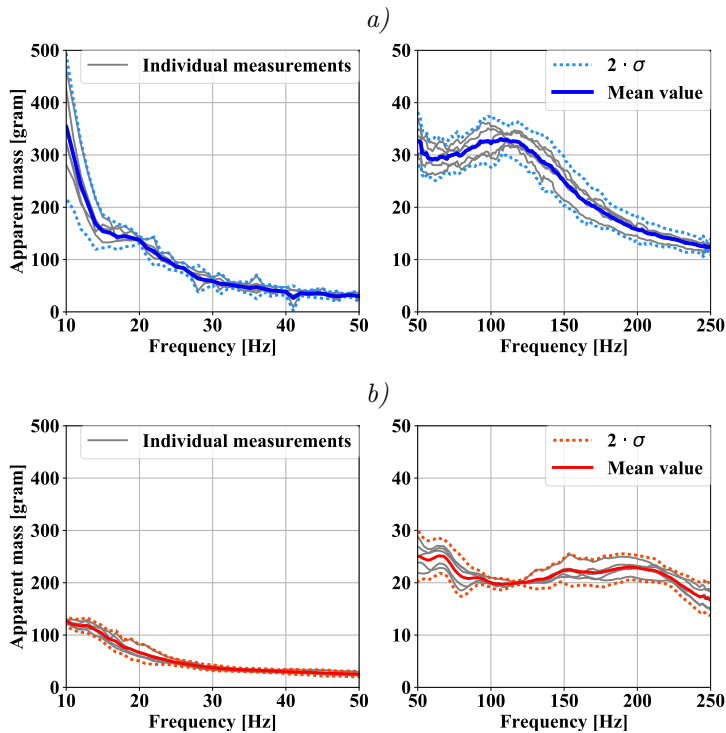


Figure 5: Repeatability of the apparent-mass magnitude measurements (σ is used for the standard deviation) obtained with: *a)* broadband random excitation and *b)* harmonic excitation. The repeatability is significantly better than the difference between the two types of excitation.

The sine-sweep apparent mass magnitude values from 10 Hz to 50 Hz are much lower than the broadband random apparent-mass magnitudes for all the excitation amplitudes (e.g., 130 g vs. 500 g) but the differences reduce with the frequency and slowly converge. The broadband random apparent-mass phase graphs exhibit a higher phase difference above 100 Hz than the harmonic graphs and the differences increase with an increase in the excitation amplitude. A narrow first peak appears at lower frequencies and the second peak is also wider for the sinusoidal excitation.

It is also evident from Figure 6 that the apparent mass magnitude is affected by the excitation amplitude. A lower acceleration amplitude corresponds to a higher apparent-mass magnitude for both types, except for minor discrepancies around 100 Hz. The acceleration dependency is not clearly evident in the phase graphs for the lower frequencies. There are, however, considerable differences above 100 Hz for the broadband random excitation.

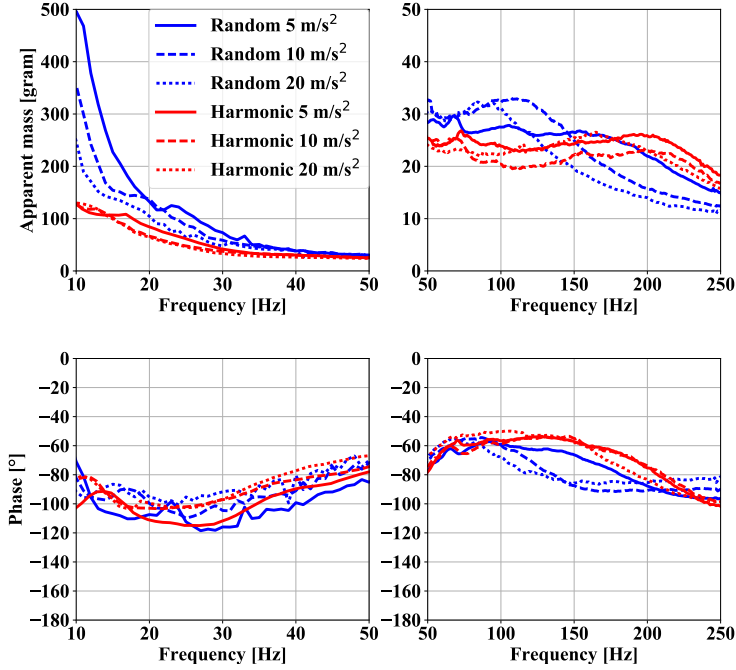


Figure 6: Index finger’s apparent mass magnitude and the phase for different excitation amplitudes. Amplitudes during random excitation are significantly higher than those during harmonic excitation.

4.2. The effects of sweep rates

The influence of the sweep rate on the measured apparent mass was researched in this section. As shown in Figure 7 the harmonic apparent mass was measured at three different sweep rates (2 oct/min, 4 oct/min and 8 oct/min) and compared to the broadband random apparent mass. The RMS acceleration value for both types of excitation was 10 m/s^2 and the finger’s push force was 5 N.

The broadband random apparent-mass magnitude values are higher up to 150 Hz compared to the harmonic excitation, with major deviations (120 g vs. 350 g) in the lower frequencies. The 4 oct/min and 8 oct/min sweep-rate-magnitude graphs overlap and exhibit lower values compared to the 2 oct/min up to 40 Hz, at which point all three sine-sweep graphs overlap. A phase lag between the broadband random apparent mass and the harmonic apparent mass is visible above 100 Hz. The second peak of the sinusoidal excitation appears at higher frequencies than the broadband random peak and is also wider. The 4 oct/min and 8 oct/min phase graphs again overlap and have a slightly lower phase shift compared to the 2 oct/min data.

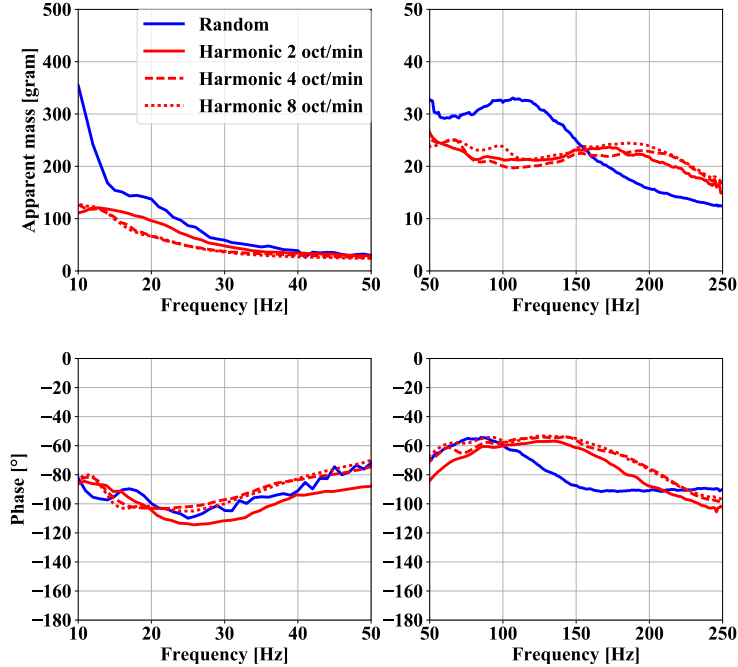


Figure 7: Index finger apparent-mass magnitude and phase for different sweep rates. The sweep rate does not significantly influence the apparent mass.

4.3. The push force compared to random and harmonic excitation

The influence of the push force on the measured apparent mass for broadband random excitation at 10 m/s^2 RMS acceleration is shown in Figure 8. The push force varied from 2 N to 10 N with a 1 N step and an additional measurement was made at 15 N.

As shown in Figure 8 an increase in the push force increases the values of the apparent mass magnitudes, especially in the lower frequencies from 10 Hz to 50 Hz. The increase in the push force also moves the entire magnitude graph to higher frequencies. The apparent-mass phase graphs are affected in a similar manner as the magnitudes: the peaks tend to move to higher frequencies and the phase seems to plateau with an increase in the push force.

The push-force effect at a harmonic excitation of 10 m/s^2 RMS acceleration amplitude and 4 oct/min sweep rate is shown in Figure 9.

Similarly, as during random excitation, the peaks move to higher frequencies if compared to Figure 8. The phase results also show an increase in the phase lag (-120° compared to -80°) in the lower frequencies due to the higher push force and the phase values are lower compared to the broadband random excitation.

In Figure 10 the random and harmonic excitation (10 m/s^2 RMS acceleration and 4 oct/min sweep-rate) for selected push forces (2 N, 5 N, 10 N) are shown

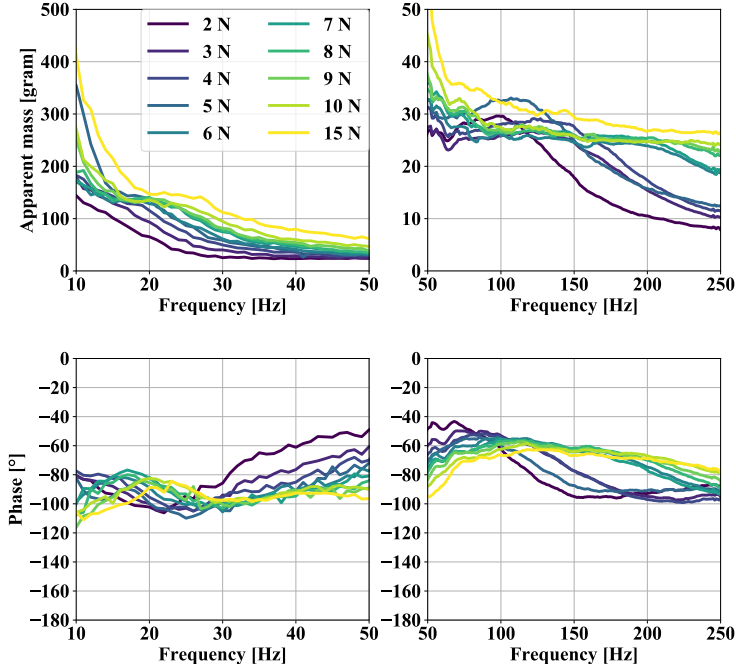


Figure 8: Index finger apparent mass magnitude and phase for broadband random excitation at different push forces. The higher the push force, the higher the amplitude of the apparent mass (especially at low below 30 Hz and above 100 Hz).

for an easier comparison of the excitation type .

5. Discussion

A direct comparison with other studies proved difficult since the closest research is on the sum of the biodynamic responses of all five fingers, whereas in this study we focused on a single finger. The apparent mass magnitudes of the finger tend to fall with an increase in the frequency and two peaks are visible. This is, in general, comparable to the findings of [12] and [13].

The apparent mass was shown to vary due to the excitation type used in the measurement (Figure 6). Considerable deviations have been observed in the 10 Hz to 30 Hz frequency range for the magnitude and above 100 Hz for the phase. These deviations are especially important for developers of tools with harmonic excitation characteristics and provide a better understanding of the threat of vibration to the fingers. The majority of hand-held tools operate in the frequency range from 10 Hz to 500 Hz, but the dominant components of vibration for vibration-induced injuries lie below 250 Hz [27]. This research shows that in the range of 10 Hz to 30 Hz the vibration input (measured via the apparent mass) into the human index finger is significantly larger than at higher

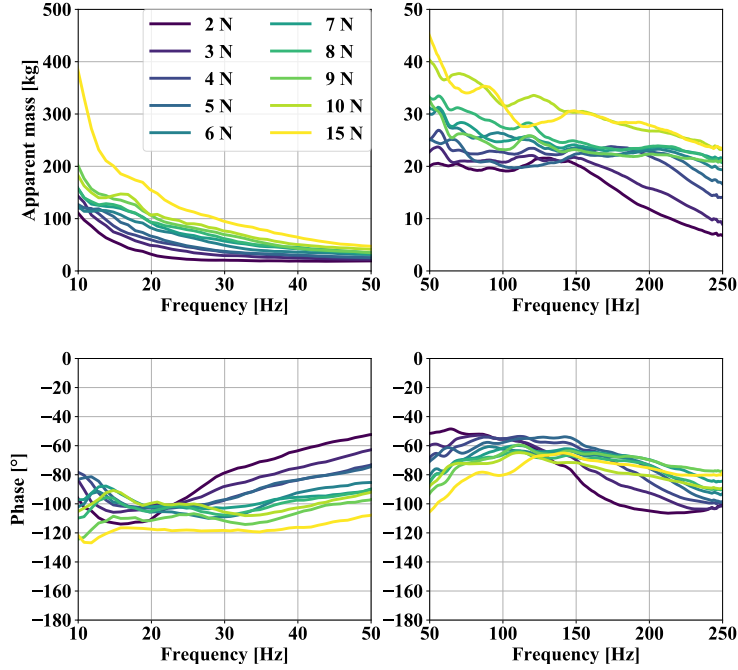


Figure 9: Index finger’s apparent-mass magnitude and the phase for harmonic excitation at different push forces. The higher the push force, the higher the amplitude of the apparent mass; significant changes are also observed in the phase response.

frequencies. If the harmonic excitation is compared to the broadband random excitation, then the apparent mass was up to 3 times larger.

Here, the excitation amplitude was found to influence the apparent mass. A lower acceleration amplitude resulted in higher apparent-mass magnitudes and also in wider phase peaks for the broadband random excitation (Figure 6). This is comparable to the research of Marcotte *et al.* [3], who found that an increase in the random excitation amplitude reduced the peak mechanical impedance amplitude and the corresponding frequency of the human hand-arm system.

The sweep-rate analysis (Figure 7) revealed that a slower 2 oct/min sweep rate provided slightly higher apparent-mass amplitudes below 40 Hz. No significant influence of the sweep rate on the apparent mass was found.

The relationship between the push force and the apparent mass (see Figures 8 and 9) for both excitation types can be explained by changes in the stiffness of the finger tissue. As the push force exerted by the index finger increases, the muscles in the finger contract. This results in higher stiffness [29], which also affects the natural frequency response of the finger.

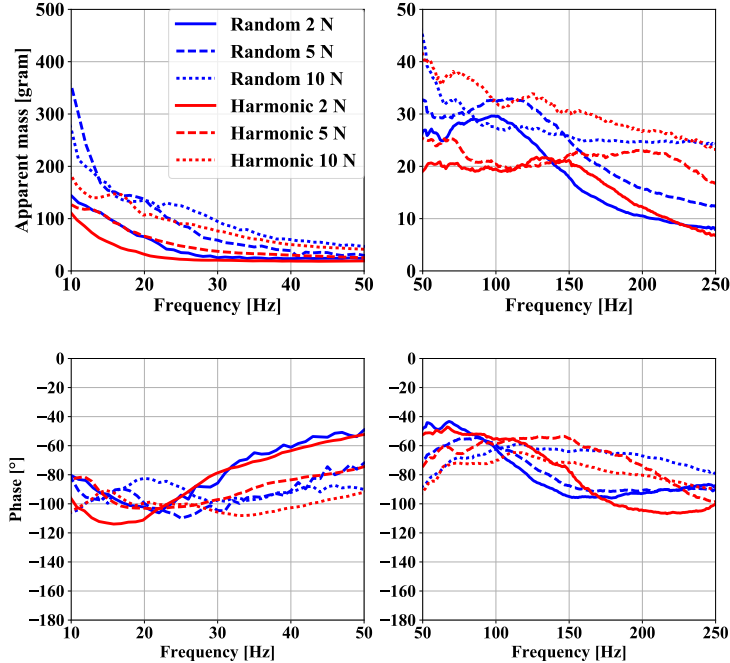


Figure 10: Index finger's apparent-mass magnitude and phase comparison for harmonic and random excitation at selected push forces. Random excitation, in general, results in a larger apparent mass.

6. Conclusions

This research is focused on the effect of vibration input to a finger during random versus harmonic excitation. It was found that for the same person significantly different vibration input is observed: the largest differences were found in the range 10–30 Hz, where the apparent-mass amplitude was up to 3 times larger during random excitation than during harmonic excitation. At frequencies of 200–250 Hz the harmonic excitation resulted in an apparent-mass amplitude slightly higher than during random excitation.

When the amplitude of the excitation was researched, the apparent-mass amplitude during random excitation was found to decrease by approximately 50% when the RMS amplitude increased by 200%. On the other hand, the 200% of excitation amplitude increase during harmonic excitation resulted in relatively small changes in the apparent mass amplitude. At 20 m/s² RMS of random excitation, the apparent-mass amplitude is still approximately two times larger than the apparent mass at 5 m/s² RMS harmonic excitation; however, with the increasing of the random excitation amplitude, the apparent mass tends to converge to the values measured during harmonic excitation.

For harmonic excitation the sweep-sine excitation was used. It was shown

that for a typically used sweep-sine rate from 2 to 8 octaves per minute the apparent mass is not significantly influenced (not in amplitude, not in phase)

The push force applied via the index finger significantly influences the identified apparent mass. In the range 10–30 Hz the apparent-mass amplitude during random excitation was found to be approximately twice the one measured with harmonic excitation. At the higher frequencies (above 200 Hz) the difference is smaller, but harmonic excitation can result in higher amplitudes of the apparent mass if compared to random excitation for the same push force.

Hand tools are frequently excited with a single or multiple harmonics, and this research compares the importance of harmonic excitation versus random excitation. Significant differences in the measured apparent mass were found if the harmonic excitation was compared to the random excitation. The identified differences could help to design safer hand tools.

Acknowledgements

This research did not receive any specific grant from funding agencies in the public, commercial, or not-for-profit sectors.

References

- [1] M. J. Griffin, Handbook of Human Vibration, Academic press, London, 1990.
- [2] M. Handford, K. Lepine, K. Boccia, F. Ruddick, D. Alyeksyeyeva, A. Thompson, L. D. Holness, S. Switzer-McIntyre, Hand-arm vibration syndrome: Workers' experience with functional impairment and disability, Journal of Hand Therapy doi:10.1016/j.jht.2016.10.010.
- [3] P. Marcotte, Y. Aldien, P. É. Boileau, S. Rakheja, J. Boutin, Effect of handle size and hand-handle contact force on the biodynamic response of the hand-arm system under z(h)-axis vibration, Journal of Sound and Vibration 283 (3-5) (2005) 1071–1091. doi:10.1016/j.jsv.2004.06.007.
- [4] L. Fattorini, A. Tirabasso, A. Lunghi, R. Di Giovanni, F. Sacco, E. Marchetti, Muscular forearm activation in hand-grip tasks with superimposition of mechanical vibrations, Journal of Electromyography and Kinesiology 26 (2016) 143–148. doi:10.1016/j.jelekin.2015.10.015.
- [5] P. Forte, Identification of the hand-arm system mechanical impedance by simultaneous measurement of grip, transmitted force and acceleration with an adaptable instrumented handle, Cogent Engineering (just-accepted).
- [6] International Organization for Standardization, Geneva, Switzerland, ISO-10819, Mechanical Vibration and Shock- Hand-Arm Vibration-Method for the Measurement and Evaluation of the Vibration Transmissibility of Gloves at the Palm of the Hand (1996).
- [7] R. G. Dong, D. E. Welcome, T. W. McDowell, J. Z. Wu, Measurement of biodynamic response of human hand-arm system, Journal of Sound and Vibration 294 (4-5) (2006) 807–827. doi:10.1016/j.jsv.2005.12.047.
- [8] L. Knez, J. Slavič, M. Boltežar, A multi-axis biodynamic measuring handle for a human hand-arm system, Journal of Mechanical Engineering 59 (2) (2013) 71–80. doi:10.5545/sv-jme.2012.709.
- [9] L. M. Roseiro, M. A. Neto, A. M. Amaro, C. J. Alcoba, M. F. Paulino, Hand-arm and whole-body vibrations induced in cross motorcycle and bicycle drivers, International Journal of Industrial Ergonomics 56 (2016) 150–160. doi:10.1016/j.ergon.2016.10.008.
- [10] M. Bovenzi, Exposure-response relationship in the hand-arm vibration syndrome: an overview of current epidemiology research, International Archives of Occupational and Environmental Health 71 (1998) 509–519. doi:10.1007/s004200050316.
- [11] J. Zimmerman, J. Bain, M. Persson, D. Riley, Effects of power tool vibration on peripheral nerve endings, International Journal of Industrial Ergonomics doi:10.1016/j.ergon.2016.08.012.

- [12] R. G. Dong, D. E. Welcome, X. S. Xu, C. Warren, T. W. McDowell, J. Z. Wu, S. Rakheja, Mechanical impedances distributed at the fingers and palm of the human hand in three orthogonal directions, *Journal of Sound and Vibration* 331 (5) (2012) 1191–1206. doi:10.1016/j.jsv.2011.10.015.
- [13] E. Concettoni, M. J. Griffin, The apparent mass and mechanical impedance of the hand and the transmission of vibration to the fingers, hand, and arm, *Journal of Sound and Vibration* 325 (3) (2009) 664–678. doi:10.1016/j.jsv.2009.03.033.
- [14] L. Burström, The influence of biodynamic factors on the mechanical impedance of the hand and arm, *International Archives of Occupational Environmental Health* 69 (1997) 437–446. doi:10.1007/s004200050172.
- [15] Y. Aldien, P. Marcotte, S. Rakheja, P. É. Boileau, Influence of hand-arm posture on biodynamic response of the human hand-arm exposed to z(h)-axis vibration, *International Journal of Industrial Ergonomics* 36 (1) (2006) 45–59. doi:10.1016/j.ergon.2005.07.001.
- [16] D. E. Welcome, R. G. Dong, X. S. Xu, C. Warren, T. W. McDowell, J. Z. Wu, An examination of the vibration transmissibility of the hand-arm system in three orthogonal directions, *International Journal of Industrial Ergonomics* 45 (2015) 21–34. doi:10.1016/j.ergon.2014.11.001.
- [17] D. D. Reynolds, A study of hand vibration on chipping and grinding operators, part ii: Four-degree-of-freedom lumped parameter model of vibration response of the human hand, *Journal of Sound and Vibration* 95 (4) (1984) 499–514. doi:10.1016/0022-460X(84)90232-3.
- [18] R. Gurram, S. Rakheja, G. J. Gouw, Mechanical impedance of the human hand-arm system subject to sinusoidal and stochastic excitations, *International Journal of Industrial Ergonomics* 16 (2) (1995) 135–145. doi:10.1016/0169-8141(94)00092-H.
- [19] L. Fattorini, A. Tirabasso, A. Lunghi, R. Di Giovanni, F. Sacco, E. Marchetti, Muscular synchronization and hand-arm fatigue, *International Journal of Industrial Ergonomics* doi:10.1016/j.ergon.2016.07.009.
- [20] A. Almagirby, M. J. Carré, J. A. Rongong, A new methodology for measuring the vibration transmission from handle to finger whilst gripping, *International Journal of Industrial Ergonomics* 58 (2017) 55–61. doi:10.1016/j.ergon.2017.02.011.
- [21] S. Mallat, *A Wavelet Tour of Signal Processing*, Academic press, 1998.
- [22] T.-P. Le, P. Argoul, Modal identification using the frequency-scale domain decomposition technique of ambient vibration responses, *Journal of Sound and Vibration* 384 (2016) 325–338.

- [23] I. Tomac, Ž. Lozina, D. Sedlar, Extended morlet-wave damping identification method, *International Journal of Mechanical Sciences* doi:10.1016/j.ijmecsci.2017.01.013.
- [24] M. Mihalec, J. Slavič, M. Boltežar, Synchrosqueezed wavelet transform for damping identification, *Mechanical Systems and Signal Processing* 80 (2016) 324–334. doi:10.1016/j.ymsp.2016.05.005.
- [25] M. Boltežar, J. Slavič, Enhancements to the continuous wavelet transform for damping identifications on short signals, *Mechanical Systems and Signal Processing* 18 (5) (2004) 1065–1076. doi:10.1016/j.ymsp.2004.01.004.
- [26] D. J. Ewins, *Modal testing theory, practice and application* second edition, Research studies press ltd., Baldock, Hertfordshire, 2000.
- [27] M. J. Griffin, *Measurement, evaluation, and assessment of occupational exposures to hand-transmitted vibration*, *Occupational Environmental Medicine* 54 (1997) 73–89. doi:10.1136/oem.54.2.73.
- [28] A. Tözeren, *Human Body Dynamics: Classical Mechanics and Human Movement*, Springer, New York, USA, 2002.
- [29] S. Kihlberg, *Biodynamic response of the hand-arm system to vibration from an impact hammer and a grinder*, *International Journal of Industrial Ergonomics* 16 (1995) 1–8. doi:10.1016/0169-8141(94)00060-G.